

# Resonant Inelastic Soft X-ray Scattering and X-ray Emission Spectroscopy of Solid Proline and Proline Solutions

Frank Meyer, Dirk Hauschild, Andreas Benkert, Monika Blum, Wanli Yang, Friedrich Reinert, Clemens Heske, Michael Zharnikov,\* and Lothar Weinhardt\*



Cite This: *J. Phys. Chem. B* 2022, 126, 10185–10193



Read Online

ACCESS |

Metrics & More

Article Recommendations

Supporting Information

**ABSTRACT:** The amino group of proline is part of a pyrrolidine ring, which makes it unique among the proteinogenic amino acids. To unravel its full electronic structure, proline in solid state and aqueous solution is investigated using X-ray emission spectroscopy and resonant inelastic soft X-ray scattering. By controlling the pH value of the solution, proline is studied in its cationic, zwitterionic, and anionic configurations. The spectra are analyzed within a “building-block principle” by comparing with suitable reference molecules, i.e., acetic acid, cysteine, and pyrrolidine, as well as with spectral calculations based on density functional theory. We find that the electronic structure of the carboxyl group of proline is very similar to that of other amino acids as well as acetic acid. In contrast, the electronic structure of the amino group is significantly



different and strongly influenced by the ring structure of proline.

## 1. INTRODUCTION

Along with nucleobases, amino acids are the most important biomolecules. From over 500 different amino acids known so far,<sup>1</sup> 23 are generally described as proteinogenic since they form all peptides and proteins of living organisms. Three out of these amino acids are rather rare, while the other 20 form the building blocks of all common proteins. Amino acids are generally composed of a carboxyl group (–COOH), an amino group (–NH<sub>2</sub>), and a specific side chain, in most cases bound to the carbon atom of a CH moiety, linking the carboxyl and amino groups. Since the amino group is a strong proton acceptor and the carboxyl group is a strong proton donor, the amino acids have a zwitterionic configuration in the physiologically relevant pH region, which is also the dominating configuration for crystalline amino acids. In this configuration, the carboxyl group is deprotonated and the amino group is protonated for most of the amino acids. This ionic state of amino acids can, however, be changed by the pH value in solution, achieving an anionic character at high pH and a cationic character at low pH.

An important characteristic of amino acids is their electronic structure, which can be effectively studied by soft X-ray spectroscopies, including X-ray photoelectron spectroscopy (XPS),<sup>2–8</sup> X-ray absorption spectroscopy (XAS),<sup>9–12</sup> X-ray emission spectroscopy (XES),<sup>13,14</sup> and resonant inelastic soft X-ray scattering (RIXS).<sup>15–18</sup> These techniques, providing information on the occupied and unoccupied electronic states, can be applied not only to solid-state samples but also to solutions.<sup>17,19–24</sup> This is especially important for amino acids

since all charge configurations, affecting the electronic structure of these molecules, can be specifically studied.<sup>17</sup> The derived information can then serve as a basis for rationalizing the spectra of more complex biomolecules, such as peptides and proteins.<sup>25–29</sup>

In this context, comprehensive XAS and XES spectral libraries of the proteinogenic amino acids in the solid state,<sup>9,10,13</sup> as well as a variety of XAS, XES, and RIXS data for these molecules in solutions,<sup>17,19–24</sup> were recorded and analyzed in detail. The XAS library has served as a basis for the spectral understanding and interpretation of homo- and heteropeptides<sup>25,26</sup> and even proved useful for rationalizing the spectra of proteins.<sup>26–28</sup> The XES library (i.e., spectra obtained with nonresonant excitation) has helped to identify the specific spectral signatures of the protonated amino group and the deprotonated carboxyl group and has provided important fingerprints for the side chains of the amino acids.<sup>13</sup> The interpretation of the spectra has relied, to a large extent, on the “building-block principle”, which was shown to be applicable not only to XAS data (as generally assumed),<sup>30</sup> but to XES as well, even though some influence of neighboring groups was observed.<sup>13</sup> This result was supported by XES and

**Received:** September 14, 2022

**Revised:** November 9, 2022

**Published:** November 23, 2022



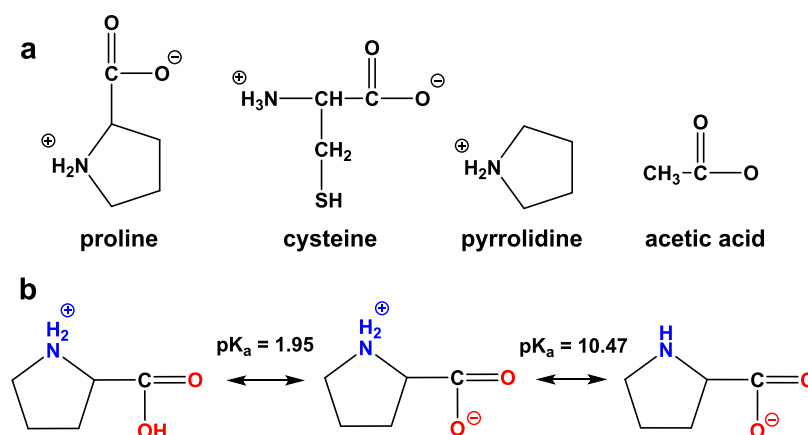


**Figure 1.** (a) Chemical structure of proline and the used reference systems (from left to right): cysteine, pyrrolidine, and acetic acid. Proline and cysteine are shown in the zwitterionic state and pyrrolidine in the cationic state. (b) All possible charge configurations of proline, together with the characteristic  $pK_a$  values for the respective transitions; the isoelectric point of proline is 6.30.<sup>31</sup>

RIXS experiments on aqueous solutions of cysteine in which the data for individual building blocks of this amino acid in specific charge configurations were compared to the analogous data for several simple reference molecules.<sup>17</sup> In view of the standard architecture of cysteine, featuring the terminal amino and carboxyl groups and a side chain, these results should also be well applicable to other amino acids with similar molecular structures.

The amino acid proline, however, differs noticeably from the others (Figure 1a). Its aliphatic side chain is back-connected to the  $\alpha$ -amino group, building a pyrrolidine ring. Due to this back connection, the amino group is in a secondary configuration instead of a primary one (as for all of the other 19 common proteinogenic amino acids). The flexibility of proline is strongly limited by this back connection, and thus it is often the cause of kinks in the structure of proteins and peptides. Due to these unique characteristics, this amino acid deserves special attention, triggering the experiments described in the present study. Within these experiments, we apply RIXS and XES to both solid-state samples and solutions of proline, specifically addressing the particular charge configurations of this molecule (Figure 1b). The results are compared with those for several reference systems (Figure 1a) and complemented by spectral calculations.

## 2. METHODS AND APPROACH

Proline and pyrrolidine were purchased from Alfa-Aesar (stated purity > 98%) as powders and used as received, without further purification. The solid-state proline samples were prepared by evaporation in high vacuum ( $10^{-6}$ – $10^{-8}$  mbar) from a Knudsen-type evaporator onto a polished copper sheet. An evaporation temperature of 413 K (140 °C) was chosen. A sufficiently large sample size was chosen ( $25 \times 12$  mm<sup>2</sup>) to ensure that multiple sample spots could be used for the RIXS measurements; this reduces the radiation dose for each particular spot. The thickness of the films was chosen at 1.2  $\mu$ m, which ensured that the substrate did not contribute to the emission signal.

To verify that the proline molecules were not destroyed during the evaporation and no contamination of the sample film occurred, the quality and stoichiometry of the samples were tested by laboratory-based XPS measurements with a Mg  $K_{\alpha}$  X-ray source and a VG CLAM 4 electron analyzer, which was calibrated according to ref 32 (see Figure S1 for the C 1s

core-level spectrum). For the RIXS studies, the samples were sealed in a dry nitrogen atmosphere and shipped to the Advanced Light Source (ALS), Lawrence Berkeley National Laboratory, where they were measured after minimal intermittent air exposure.

Furthermore, three different proline solutions with pH values of 0.8, 6.8, and 13.0, as well as two different pyrrolidine solutions with pH values of 1.4 and 13.6 were prepared and measured. The compounds were dissolved in ultrapure water and the pH value was adjusted by adding NaOH or HCl. Proline concentrations of 3 mol/L (for pH 6.8) and 2.6 mol/L (for pH 0.8 and 13.0) were used.

XES (i.e., with nonresonant excitation) and RIXS (i.e., with excitation close to the absorption edge) experiments were performed with the custom-designed Solid and Liquid Spectroscopic Analysis (SALSA) endstation<sup>33</sup> at Beamline 8.0.1 of the ALS. This endstation is equipped with a variable line space grating soft X-ray spectrometer, which is built in a slitless design and optimized for maximum transmission at the biologically relevant C, N, and O absorption K edges.<sup>34</sup> All of these edges were investigated, with particular focus on the N and O K edges for the solution samples. The high transmission of the spectrometer allows recording a single XES or RIXS spectrum with a very good signal-to-noise ratio within 30 s. For RIXS measurements, the excitation energy was varied over the absorption edges with a step size of 0.1 eV. The data is then presented in a two-dimensional map, where the X-ray emission intensity is color-coded as a function of excitation and emission energies.<sup>15,17,23</sup> In a few cases, additional RIXS spectra were measured at specific energies with higher signal-to-noise ratios. The excitation and emission energy scales were calibrated simultaneously using reference measurements and literature values for N<sub>2</sub>,<sup>35</sup> TiO<sub>2</sub>,<sup>36</sup> and HOPG.<sup>37</sup>

To avoid radiation damage, the solid-state samples were continuously moved under the beam during spectra acquisition. For the resulting exposure time of 0.17 s/sample spot, the influence of beam induced on the spectra becomes negligible, as discussed in Section 2 of the Supporting Information.

The measurements of the solutions were performed with a custom-designed flow-through liquid cell,<sup>33</sup> which is a part of SALSA. The sample liquid was separated from the vacuum of the analysis chamber by either a thin Si<sub>3</sub>N<sub>4</sub> membrane (100 nm; Silson) for the C and O K edges or a SiC membrane (100

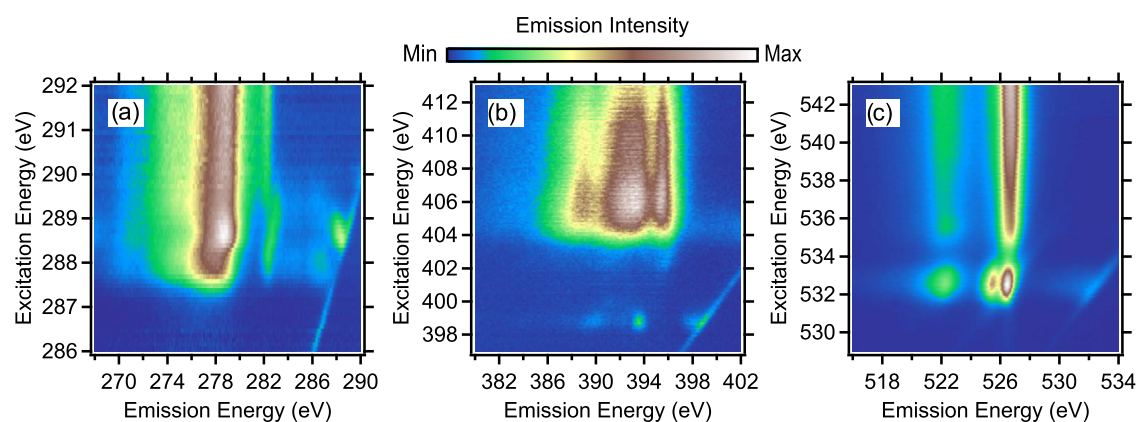


**Figure 2.** C (a), N (b), and O (c) K-edge RIXS maps of an evaporated proline film. The X-ray emission intensity is color-coded (see the scale bar above the maps) and plotted as a function of emission (abscissa) and excitation (ordinate) energies. Blue represents zero and white indicates the strongest intensity.

nm; NTT) for the N K edge. The sample liquid was continuously pumped through the cell, replacing its volume  $\sim 770$  times/s, to quickly remove X-ray-damaged molecules from the probing volume. In all measurements, we have carefully checked for contributions of damaged molecules as described in Section 2 of the Supporting Information. In most cases (with the exception of the N K RIXS data of proline at pH values of 6.8 and 13.0), spectra with no or only small signatures of damaged molecules could be collected.

Complementary to the experiments, density functional theory (DFT) calculations for proline and pyrrolidine were performed using the StoBe-deMon code.<sup>38</sup> A more detailed description can be found in ref 39.

### 3. RESULTS AND DISCUSSION

**3.1. Proline in the Solid State.** As a solid and also at a neutral pH value, proline is in the zwitterionic configuration, which corresponds to a protonated pyrrolidine moiety and a deprotonated carboxyl group, as shown in Figure 1. The C, N, and O K RIXS maps of the evaporated proline film are depicted in Figure 2. Each horizontal cut through such maps represents a single RIXS spectrum, excited with a photon energy according to the excitation axis. Vertical cuts through the maps represent partial fluorescence yield XAS spectra. The sharp diagonal lines at equal emission and excitation energies in the bottom right corner of the maps represent Rayleigh lines, i.e., caused by elastically scattered photons. For particular excitation energies, the Rayleigh lines show a resonant enhancement, which is accompanied by additional intensity at slightly lower emission energies. These result from quasi-elastic transitions, for which the final state is also the electronic ground state, but with an excited vibronic state. The bright intensity in the center of all three maps is the result of inelastic scattering processes in which the final state is an excited valence electronic state, with a “hole” in the valence orbitals and an electron in the formerly unoccupied orbitals.

The C K RIXS map of solid proline is depicted in Figure 2a. This map shows a strong excitation dependence below an excitation energy ( $E_{\text{exc}}$ ) of  $\sim 290$  eV. Above this energy, the emission spectrum no longer changes with increasing  $E_{\text{exc}}$ . The emission starts at an excitation energy of ca. 287.2 eV (in the following always referred to as “absorption onset”) and becomes strongest at an excitation energy of 288.6 eV, corresponding to the  $\pi^*(\text{COO})$  resonance.<sup>10</sup> Both at 288.0

and 288.6 eV, pronounced vibrational structures appear at and near the elastic line, indicating a strong vibronic coupling. These features originate from nuclear dynamics in the core-excited state, leading to vibronically excited states<sup>40,41</sup> or to the dissociation of the molecule<sup>41,42</sup> on the time scale of the X-ray emission process (i.e., the core–hole lifetime). Apart from the vibrational structures, the emission pattern shows a strong asymmetric feature at an emission energy ( $E_{\text{em}}$ ) of 278–279 eV and a weaker feature at 282.3–282.6 eV (see selected detailed spectra in Figure S5). The  $E_{\text{em}}$  of both features changes slightly with increasing excitation energy, starting from the absorption onset: the strongest emission shifts progressively to higher emission energies, while the weaker one shifts first to lower, then to higher, and back to lower energies (see also Figure S5). These shifts can be attributed to “spectator shifts”, i.e., changes in the final-state energy caused by the presence of the excited (spectator) electron.

The N K RIXS map of solid proline is displayed in Figure 2b. We find the absorption onset at  $E_{\text{exc}} \approx 404.0$  eV and a maximum at  $\sim 405.7$  eV that is assigned to the  $\sigma^*(\text{C–N})$  resonance.<sup>10</sup> The map exhibits three main emission features, at 389, 393, and 395.5 eV, that stay at constant emission energy over the entire excitation-energy range. The map also reveals a very small absorption resonance at  $E_{\text{exc}} = 398.8$  eV. The energy and emission signature of this resonance are very different from the “regular” N K emission pattern for amino acids,<sup>13</sup> which we attribute to a small contribution from X-ray-damaged molecules. A feature at similar energy, increasing in intensity in the course of X-ray exposure, can be found in methylammonium-containing perovskites<sup>43</sup> and glycine,<sup>44</sup> and has been attributed to the dissociation of a hydrogen atom from the amino group caused by the X-ray irradiation.

The O K RIXS map of solid proline is displayed in Figure 2c. The map exhibits a clear and well-separated absorption feature at  $E_{\text{exc}} = 532.6$  eV, assigned to the  $\pi^*(\text{COO})$  resonance.<sup>10</sup> At this resonance, we find the very characteristic fingerprint of the deprotonated carboxyl group, consisting of three well-separated emission features at 526.5, 525.4, and 522.3 eV.<sup>17,21</sup> These peaks can be assigned to the lone-pair (526.5 and 525.4 eV) and lower-lying (522.3 eV) orbitals.<sup>21</sup> For excitation energies higher than 535 eV, the lone-pair peaks merge into one emission line at 526.7 eV with a weak shoulder at low emission energies, giving the typical emission fingerprint observed for solid (i.e., zwitterionic) amino acids upon

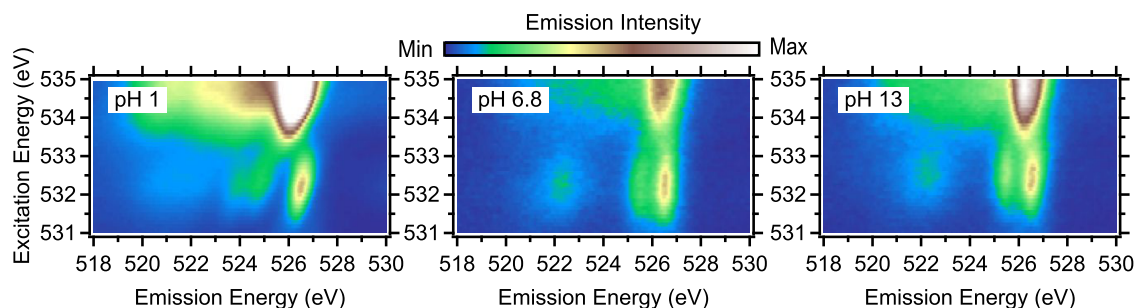


**Figure 3.** O K RIXS maps of proline in aqueous solutions at three different pH values (0.8, 6.8, and 13.0), representing the cationic, zwitterionic, and anionic configurations. The absorption onset of water is visible in the top part of the maps. The X-ray emission intensity is color-coded, as given by the scale bar above the maps.

nonresonant excitation.<sup>13</sup> These excitation-energy-dependent changes can be attributed to spectator shifts, as well as to changes in relative emission intensities caused by the angular anisotropy of the X-ray emission process.<sup>45</sup>

**3.2. Proline Solution: O K Edge.** For the carboxyl group of proline, the  $pK_a$  value of 1.97 is below the average  $pK_a$  value found for other amino acids. The  $pK_a$  value of the carboxyl group is influenced by the neighboring amino group and thus varies between different amino acids. Here, the smaller  $pK_a$  value can be interpreted as a larger influence of the pyrrolidine ring on the carboxyl group.<sup>46</sup>

Figure 3 shows the O K RIXS maps of proline in aqueous solutions at three different pH values. The absorption edge of water starts at  $E_{exc} \sim 534$  eV<sup>15,47</sup> and then dominates the maps. For energies below the absorption onset of water, it is completely transparent, and thus the emission features can be exclusively related to the carboxyl group of proline. As expected, the pre-edges of the maps for the zwitterionic (pH 6.8) and anionic (pH 13.0) configurations of proline are nearly identical and show the three proline-related emission features (at 522.3, 525.4, and 526.5 eV) typical of the deprotonated carboxyl group. This is in accordance with the solid-state data for proline (Figure 2c) and previous experiments on glycine,<sup>48</sup> cysteine,<sup>17</sup> and acetic acid.<sup>21</sup> Similar to acetic acid, the  $\pi^*(COO)$  absorption resonance is found at  $E_{exc} = 532.5$  eV.<sup>21</sup> For the neutral carboxyl group (pH 0.8), we find a small shift of 0.3 eV to lower  $E_{exc}$ , which agrees well with the one found for acetic acid when going from high to low pH.<sup>21</sup> At pH 0.8, the emission fingerprint is distinctly different, featuring a strong peak at  $E_{em} = 526.5$  eV and three additional (weak) peaks at  $E_{em}$  of 524.8, 524.0, and  $\sim 521$  eV. This emission pattern is in good agreement with the analogous data for cysteine<sup>17</sup> and acetic acid<sup>21,49,50</sup> at low pH. The dominating peak at 526.5 eV can be attributed to the lone-pair orbital at the double-bonded oxygen,<sup>21</sup> while the peaks at lower energies are related to less localized orbitals.<sup>21</sup>

For a closer inspection of the O K RIXS fingerprints for different proline configurations, the RIXS spectra extracted from the maps are compared with the spectra of solid proline and acetic acid with either the protonated (pH 0.2) or deprotonated (pH 12.8) carboxyl group (Figure 4). The spectra confirm the energies of all emission features of proline as they were assigned above. Furthermore, two more details become visible. First, the low-energy feature ( $E_{em} = 520$ – $523$  eV) of the cationic proline (pH 0.8) shows a distinct asymmetry and fine structure, indicating that the observed intensity is the result of multiple transitions. Second, the spectra of zwitterionic (pH 6.8) liquid, solid, and anionic (pH

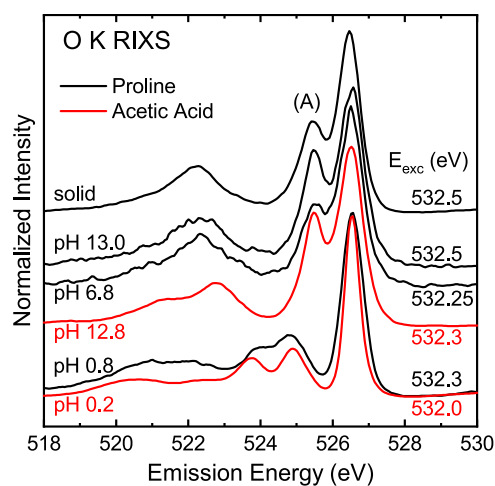


**Figure 4.** O K RIXS spectra of proline (black curves) in aqueous solution at various pH values (0.8, 6.8, and 13.0), representing its cationic, zwitterionic, and anionic configurations. For comparison, the spectra of solid proline (black, top) and acetic acid (red curves) at pH 0.2 and 12.8 (taken from ref 17) are also shown. The acetic acid spectra were aligned with the proline spectra (shifted by +0.3 eV in emission energy). The low pH spectra represent a neutral carboxyl group, while the neutral and high-pH solutions correspond to a deprotonated carboxyl group (see Figure 1b). The spectra of proline were extracted from the RIXS maps in Figure 3.

13.0) proline are similar but not identical. The anionic configuration at pH 13.0 exhibits a higher intensity of feature (A) as compared to the zwitterionic configurations and agrees very well with the spectral shape found for acetic acid (pH 12.8).<sup>17</sup> In comparison, the relative intensity of feature (A) is lower for the zwitterionic solid sample and even lower for zwitterionic proline in aqueous solution. This shows that the emission of the lone-pair orbitals is sensitive to both the charge state of the proline (zwitterionic vs anionic) as well as to the environment of the molecule (solvation vs solid state).

Apart from the discussed details, a good similarity of the spectra of proline in the cationic and anionic configurations and acetic acid with the protonated or deprotonated carboxyl group implies the validity of the building-block principle in the case of proline, similar to other amino acids.<sup>17</sup> In this context, the O K RIXS spectra of proline can also be compared to the analogous spectra of other amino acids. In particular, the data for zwitterionic glycine<sup>22,48</sup> and cysteine<sup>17</sup> show large similarities to those for zwitterionic proline.

**3.3. Proline Solution: N K Edge.** The N K RIXS map of proline representing the cationic (pH 0.8) configuration is

shown in Figure 5, while no corresponding maps for the zwitterionic and anionic states could be collected without

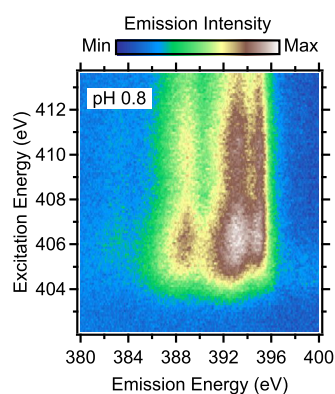


**Figure 5.** N K RIXS map of proline in aqueous solution at pH 0.8 representing the cationic configuration. The X-ray emission intensity is color-coded, as given by the scale bar above the map.

contributions of damaged molecules adsorbed on the membrane (see Section 2 of the Supporting Information). The N K RIXS map of the cationic configuration fits to the respective RIXS map of solid proline (Figure 2b), representing the protonated pyrrolidine ring as well (see Figure 1b).

In the following, we will discuss the nonresonantly excited N K XES spectra of all configurations of proline, collected on fresh spots of the membrane with an acquisition time sufficiently short to minimize the X-ray-induced damage associated with the decomposition of proline (see also discussion in Section 2 of the Supporting Information). The spectra are depicted in Figure 6. As expected, the spectra of the cation (pH 0.8) and zwitterion (pH 6.8) configurations are very similar since the pyrrolidine ring is protonated ( $\text{NH}_2^+$ ) at both pH values. In contrast, the pH 13.0 solution shows the spectrum of the anionic proline, which hosts a neutral pyrrolidine ring. These spectra can be compared with the

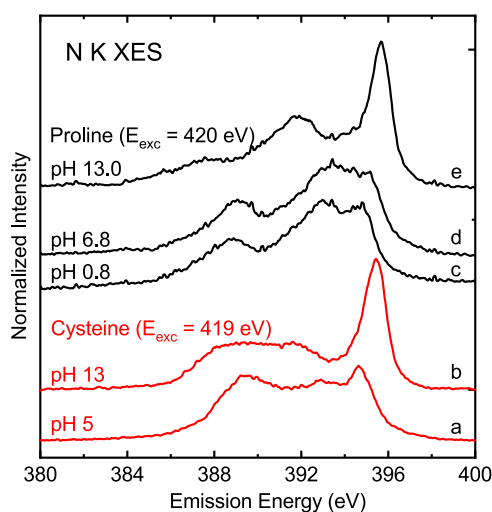


**Figure 6.** Nonresonant ( $E_{\text{exc}} = 419$  eV) N K XES spectra of proline in aqueous solution at various pH values (0.8, 6.8, and 13.0) representing the cationic (c), zwitterionic (d), and anionic (e) configurations. For comparison, nonresonant ( $E_{\text{exc}} = 420$  eV) N K XES spectra of cysteine in zwitterionic (a) and anionic (b) configurations are shown (first published in ref 17).

analogous spectra of zwitterionic (pH 5) and anionic (pH 13) cysteine,<sup>17</sup> which are also included in Figure 6. The latter spectra show the typical fingerprints of a protonated ( $\text{NH}_3^+$ ) and neutral  $\alpha$ -amino group, respectively.<sup>13,23,51</sup>

The N K XES spectra of the cationic and zwitterionic proline are, except for a small energy shift of about 0.3 eV, identical, exhibiting three emission features centered at an  $E_{\text{em}}$  of 388.8, 393.0, and 394.7 eV. The energy shift might be an indicator for the changes at the carboxyl group (neutral vs deprotonated), leading to some charge redistribution over the molecule, which slightly changes the N 1s binding energy. The observed emission spectrum is distinctly different from that of zwitterionic cysteine. This can be related to the significantly different backbone of these two amino acids and to the fact that for a protonated amino group, mainly emission from orbitals with significant overlap with this backbone contributes to the spectrum.<sup>23</sup> For protonated amino groups in primary configuration (like cysteine), it was shown that ultrafast proton dynamics on the time scale of the X-ray emission process significantly influence the spectral shape and give rise to the peak observed at 394.6 eV. Whether this is that case for proline will be discussed below, in connection with the comparison with pyrrolidine solutions and calculated spectra.

As expected, the spectrum of anionic proline (pH 13.0) has a completely different spectral signature than the spectra of its zwitterionic and cationic configurations. This spectrum consists of a strong and sharp emission at 395.7 eV and two weaker and broader emission features at 391.8 and 387.5 eV. The latter feature is very broad and has a low-energy tail that extends to 383.9 eV. The spectrum of anionic cysteine is also dominated by a high-energy feature, with the peak shape, relative intensity, and energy position being nearly identical to those for proline. Analogous to glycine<sup>22</sup> and cysteine,<sup>17</sup> this feature is assigned to the lone-pair orbital of the nitrogen atom of proline.

The low-energy part of the spectrum is, however, distinctly different. This region is again dominated by contributions from orbitals with significant overlap with the molecular backbone, which is very different for proline with its ring structure.

The N K XES and RIXS data of proline were compared to those of pyrrolidine, which is the main building block of proline (see Figure 1). The N K RIXS maps of protonated (pH 1.4) and neutral (pH 13.6) pyrrolidine in aqueous solution are shown in Figure 7 (see Figure S6 for the corresponding XES and XAS spectra). The maps of proline and pyrrolidine, representing the protonated pyrrolidine ring, are very similar, suggesting large similarities between the electronic structure of proline and pyrrolidine in the direct vicinity of the nitrogen atom. The map of the neutral configuration of pyrrolidine could not be compared to the map of the anionic configuration of proline, since the latter map was affected by beam-induced decomposition and subsequent fragment adsorption on the membrane (see above). The map of pyrrolidine seems to be much less (if at all) affected by these effects, suggesting that pyrrolidine is more robust under soft X-ray exposure than proline.

The spectra extracted from the N K RIXS maps of pyrrolidine (red) can be compared to the N K-edge XES spectra of proline (black) in Figure 8. We find a good correlation between the spectra of these two molecules. The XES spectrum of the neutral pyrrolidine (pH 13.6) has a very similar shape to that of anionic proline (pH 13.0). This spectrum exhibits four spectral features centered at  $E_{\text{em}} =$

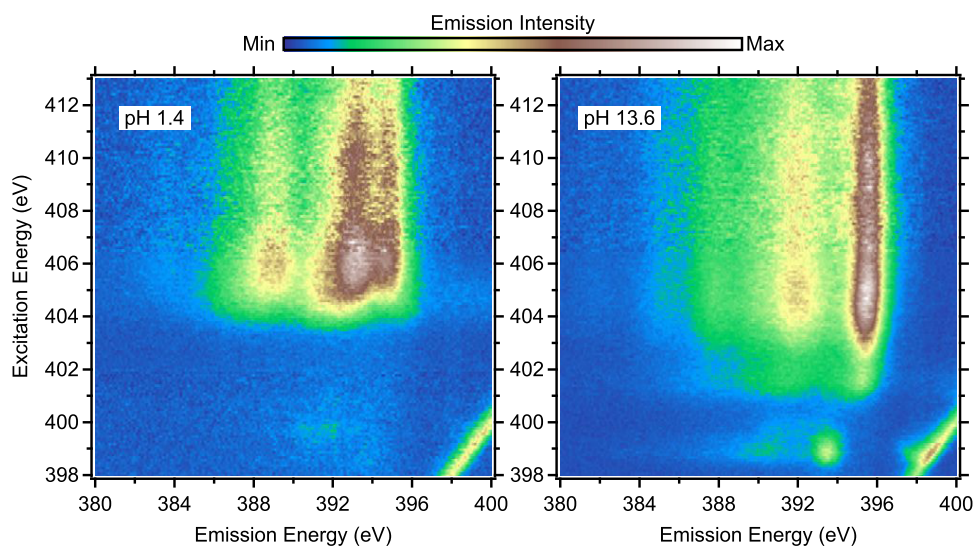


**Figure 7.** N K-edge RIXS maps of pyrrolidine in aqueous solution at pH 1.4 and 13.6, representing the cationic and neutral configurations, respectively. The X-ray emission intensity is color-coded, as shown in the scale bar above the maps.

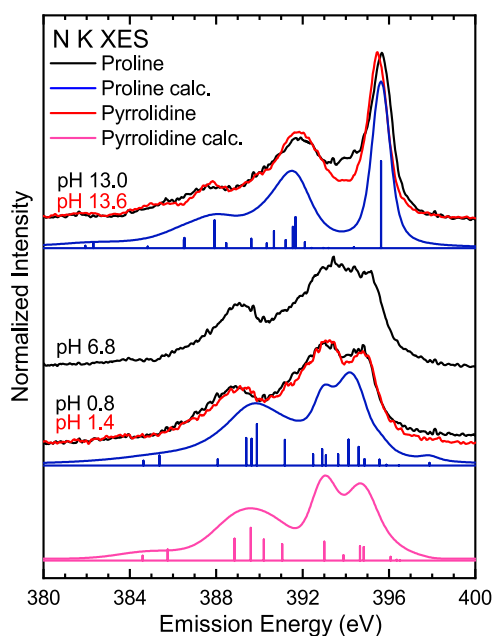


**Figure 8.** Nonresonant N K-edge XES spectra of proline (black curves,  $E_{\text{exc}} = 419$  eV) and pyrrolidine (red curves,  $E_{\text{exc}} = 424$  eV) in aqueous solution at pH values corresponding to the cationic (pH 0.8 and 1.4, resp.), zwitterionic (pH 6.8), and anionic (pH 13.0 and 13.6, resp.) configurations. The spectra of pyrrolidine were extracted from the RIXS maps in Figure 7. The experimental data are complemented by the calculated X-ray emission energy positions and intensities of isolated cationic and neutral proline (blue bars). The calculation for an isolated protonated pyrrolidine ion is shown in magenta. The blue and magenta curves were derived by applying a Gaussian broadening for which the FWHM was increased at lower emission energies.

395.5, 391.8, 397.8, and 385.1 eV. Similarly, the spectrum of protonated pyrrolidine (pH 1.4) is nearly identical to that of cationic proline (pH 0.8). The spectrum exhibits three overlapping peaks, with the most intense emission feature located at  $E_{\text{em}} = 394.8$  eV and two less intense features located at 393.2 and 389.1 eV.

Additional information, especially for the highest occupied molecular orbitals (HOMOs), can be gained by comparing the

experimental and theoretical spectra, the latter being calculated for isolated proline and pyrrolidine molecules (see Section 2 for technical details). Calculated emission energies, weighted by the respective oscillator strengths, are depicted in Figure 8 for the protonated and deprotonated configurations of proline (blue) as well as the protonated configuration of pyrrolidine (magenta). We find that the agreement between theory and experiment for the deprotonated configuration is, in general, very good. However, the calculated spectrum shows no intensity at  $E_{\text{em}} = 394.0$  eV, while the experiment still exhibits a noticeable signal in this region. This discrepancy might be caused by the environment of the molecule (e.g., hydrogen bonds between the amino group and water molecules<sup>52</sup>); also, a contribution from molecular fragments adsorbed on the membrane cannot be ruled out. Regardless of these differences, the calculations allow assigning the dominant feature in the N K-edge XES spectrum to the HOMO of this molecule, i.e., the lone-pair orbital at the nitrogen atom. The weaker features at lower emission energies are then assigned to a number of orbitals that have a strong overlap with the backbone of the molecule.

For proline with a protonated amino group, the agreement between the calculation and experiment is not as good, while the overall spectral shape is better reproduced in the case of pyrrolidine, albeit with a compressed energy scale. We note that the calculations for protonated proline and pyrrolidine differ in the region between 392 and 396 eV, which can possibly be explained by the influence of the carboxyl group for proline. It is expected to have a much stronger effect for an isolated ion, while its influence is strongly reduced in solution, i.e., by interacting with the solvation shell. We also note that for both calculations, the relative intensity in the region between 392 and 396 eV is lower than in the experiment. This might be an indication that, similar to the case with amino groups in primary configuration, proton dynamics on the time scale of the X-ray emission process play a role,<sup>23</sup> which is not included in the calculations.

#### 4. CONCLUSIONS

The RIXS maps and XES spectra of proline as solid and in aqueous solutions have been compared with data of several

reference systems, with particular emphasis on pyrrolidine. While the data for solid proline correspond to the zwitterionic configuration of this molecule, the measurements in solution allow access to all three charge states of proline (cation, anion, zwitterion) by adjusting the solution's pH value. The spectral signature of both the carboxyl group and the pyrrolidine ring of proline were found to be strongly influenced by their protonation and deprotonation. The data can be well understood within the building-block principle, comparing with acetic acid and pyrrolidine as reference systems. We find a good agreement between the maps and spectra of proline and the reference systems for all charge configurations, with only a small influence by the neighboring groups. At the same time, the unique pyrrolidine building block of proline, differing from the  $\alpha$ -amino group of other amino acids, results in unique N K-edge XES spectra, with only some similarity to the spectra of other amino acids (such as cysteine). Additional insight is gained by comparing the experimental data with theoretical (DFT) simulations that allow the assignment of individual emission features to specific molecular orbitals.

## ■ ASSOCIATED CONTENT

### SI Supporting Information

The Supporting Information is available free of charge at <https://pubs.acs.org/doi/10.1021/acs.jpcc.2c06557>.

Discussion of the quality of the evaporated proline film, discussion of the influence of beam-induced fragmentation on the spectra, data of spectator shifts in the C K RIXS of solid proline, and N K XES and XAS of aqueous pyrrolidine (PDF)

## ■ AUTHOR INFORMATION

### Corresponding Authors

**Michael Zharnikov** – Applied Physical Chemistry, Heidelberg University, 69120 Heidelberg, Germany; [orcid.org/0000-0002-3708-7571](https://orcid.org/0000-0002-3708-7571); Email: [Michael.Zharnikov@urz.uni-heidelberg.de](mailto:Michael.Zharnikov@urz.uni-heidelberg.de)

**Lothar Weinhardt** – Department of Chemistry and Biochemistry, University of Nevada, Las Vegas (UNLV), Las Vegas, Nevada 89154-4003, United States; Institute for Photon Science and Synchrotron Radiation (IPS), Karlsruhe Institute of Technology (KIT), 76344 Eggenstein-Leopoldshafen, Germany; Institute for Chemical Technology and Polymer Chemistry (ITCP), Karlsruhe Institute of Technology (KIT), 76128 Karlsruhe, Germany; [orcid.org/0000-0003-3361-1054](https://orcid.org/0000-0003-3361-1054); Email: [Lothar.Weinhardt@kit.edu](mailto:Lothar.Weinhardt@kit.edu)

### Authors

**Frank Meyer** – Experimentelle Physik VII, Universität Würzburg, 97074 Würzburg, Germany; Present Address: Fraunhofer-Institut für Werkstoffmechanik (IWM), Wöhlerstraße 11, 79108 Freiburg, Germany

**Dirk Hauschild** – Department of Chemistry and Biochemistry, University of Nevada, Las Vegas (UNLV), Las Vegas, Nevada 89154-4003, United States; Institute for Photon Science and Synchrotron Radiation (IPS), Karlsruhe Institute of Technology (KIT), 76344 Eggenstein-Leopoldshafen, Germany; Institute for Chemical Technology and Polymer Chemistry (ITCP), Karlsruhe Institute of Technology (KIT), 76128 Karlsruhe, Germany; [orcid.org/0000-0001-9088-8944](https://orcid.org/0000-0001-9088-8944)

**Andreas Benkert** – Experimentelle Physik VII, Universität Würzburg, 97074 Würzburg, Germany; Institute for Chemical Technology and Polymer Chemistry (ITCP), Karlsruhe Institute of Technology (KIT), 76128 Karlsruhe, Germany

**Monika Blum** – Department of Chemistry and Biochemistry, University of Nevada, Las Vegas (UNLV), Las Vegas, Nevada 89154-4003, United States; Advanced Light Source (ALS), Lawrence Berkeley National Laboratory, Berkeley, California 94720, United States; Chemical Sciences Division, Lawrence Berkeley National Laboratory, Berkeley, California 94720, United States; [orcid.org/0000-0002-2918-9092](https://orcid.org/0000-0002-2918-9092)

**Wanli Yang** – Advanced Light Source (ALS), Lawrence Berkeley National Laboratory, Berkeley, California 94720, United States; [orcid.org/0000-0003-0666-8063](https://orcid.org/0000-0003-0666-8063)

**Friedrich Reinert** – Experimentelle Physik VII, Universität Würzburg, 97074 Würzburg, Germany

**Clemens Heske** – Department of Chemistry and Biochemistry, University of Nevada, Las Vegas (UNLV), Las Vegas, Nevada 89154-4003, United States; Institute for Photon Science and Synchrotron Radiation (IPS), Karlsruhe Institute of Technology (KIT), 76344 Eggenstein-Leopoldshafen, Germany; Institute for Chemical Technology and Polymer Chemistry (ITCP), Karlsruhe Institute of Technology (KIT), 76128 Karlsruhe, Germany; [orcid.org/0000-0001-7586-4549](https://orcid.org/0000-0001-7586-4549)

Complete contact information is available at:

<https://pubs.acs.org/doi/10.1021/acs.jpcc.2c06557>

### Notes

The authors declare no competing financial interest.

## ■ ACKNOWLEDGMENTS

This work was supported by the German Research Society (DFG; Project Nos. RE 1469/7-1 and ZH 63/16-1). This research used resources of the Advanced Light Source, a U.S. DOE Office of Science User Facility under Contract No. DE-AC02-05CH11231.

## ■ REFERENCES

- (1) Wagner, I.; Musso, H. New Naturally Occurring Amino Acids. *Angew. Chem., Int. Ed.* **1983**, *22*, 816–828.
- (2) Zubavichus, Y.; Fuchs, O.; Weinhardt, L.; Heske, C.; Umbach, E.; Denlinger, J. D.; Grunze, M. Soft X-Ray-Induced Decomposition of Amino Acids: An XPS, Mass Spectrometry, and NEXAFS Study. *Radiat. Res.* **2004**, *161*, 346–358.
- (3) Cavalleri, O.; Gonella, G.; Terreni, S.; Vignolo, M.; Floreano, L.; Morgante, A.; Canepa, M.; Rolandi, R. High Resolution X-ray Photoelectron Spectroscopy of L-Cysteine Self-Assembled Films. *Phys. Chem. Chem. Phys.* **2004**, *6*, 4042–4046.
- (4) Plekan, O.; Feyrer, V.; Richter, R.; Coreno, M.; de Simone, M.; Prince, K. C.; Carravetta, V. Investigation of the Amino Acids Glycine, Proline, and Methionine by Photoemission Spectroscopy. *J. Phys. Chem. A* **2007**, *111*, 10998–11005.
- (5) Kamada, M.; Sugiyama, H.; Takahashi, K.; Azuma, J.; Kitajima, S.; Ogawa, K.; Sumimoto, M.; Hori, K.; Fujimoto, H. Photoelectron Spectroscopic Study of Electronic Structures of L-Cysteine. *J. Phys. Soc. Jpn.* **2010**, *79*, No. 034709.
- (6) Ataman, E.; Isvoranu, C.; Knudsen, J.; Schulte, K.; Andersen, J. N.; Schnadt, J. Adsorption of L-Cysteine on Rutile TiO<sub>2</sub>(110). *Surf. Sci.* **2011**, *605*, 179–186.
- (7) Kostko, O.; Xua, B.; Ahmedet, M. Local electronic structure of histidine in aqueous solution. *Phys. Chem. Chem. Phys.* **2021**, *23*, 8847.

- (8) Stevens, J. S.; de Luca, A. C.; Pelendritis, M.; Terenghi, G.; Downes, S.; Schroeder, S. L. M. Quantitative analysis of complex amino acids and RGD peptides by X-ray photoelectron spectroscopy (XPS). *Surf. Interface Anal.* **2013**, *45*, 1238.
- (9) Kaznacheyev, K.; Osanna, A.; Jacobsen, C.; Plashkevych, O.; Vahtras, O.; Ågren, H.; Carravetta, V.; Hitchcock, A. P. Inner-shell Absorption Spectroscopy of Amino Acids. *J. Phys. Chem. A* **2002**, *106*, 3153–3168.
- (10) Zubavichus, Y.; Shaporenko, A.; Grunze, M.; Zharnikov, M. Inner-shell Absorption Spectroscopy of Amino Acids at All Relevant Absorption Edges. *J. Phys. Chem. A* **2005**, *109*, 6998–7000.
- (11) Plekan, O.; Feyer, V.; Richter, R.; Coreno, M.; de Simone, M.; Prince, K.; Carravetta, V. An X-ray Absorption Study of Glycine, Methionine and Proline. *J. Electron Spectrosc. Relat. Phenom.* **2007**, *155*, 47–53.
- (12) Buckley, M. W.; Besley, N. A. A Theoretical Study of the Near Edge X-ray Absorption Fine Structure of Amino Acids and Proteins. *Chem. Phys. Lett.* **2011**, *501*, 540–546.
- (13) Meyer, F.; Blum, M.; Benkert, A.; Hauschild, D.; Jeyachandran, Y. L.; Wilks, R. G.; Yang, W.; Bär, M.; Heske, C.; Reinert, F.; et al. X-ray Emission Spectroscopy of Proteinogenic Amino Acids at All Relevant Absorption Edges. *J. Phys. Chem. B* **2017**, *121*, 6549–6556.
- (14) Horikawa, Y.; Tokushima, T.; Takahashi, O.; Harada, Y.; Hiraya, A.; Shin, S. Effect of Amino Group Protonation on the Carboxyl Group in Aqueous Glycine Observed by O 1s X-Ray Emission Spectroscopy. *Phys. Chem. Chem. Phys.* **2018**, *20*, 23214.
- (15) Weinhardt, L.; Fuchs, O.; Blum, M.; Bär, M.; Weigand, M.; Denlinger, J. D.; Zubavichus, Y.; Zharnikov, M.; Grunze, M.; Heske, C.; Umbach, E. Resonant X-Ray Emission Spectroscopy of Liquid Water: Novel Instrumentation, High Resolution, and the “Map” Approach. *J. Electron Spectrosc. Relat. Phenom.* **2010**, *177*, 206–211.
- (16) Meyer, F.; Weinhardt, L.; Blum, M.; Bär, M.; Wilks, R. G.; Yang, W.; Heske, C.; Reinert, F. Non-Equivalent Carbon Atoms in the Resonant Inelastic Soft X-ray Scattering Map of Cysteine. *J. Chem. Phys.* **2013**, *138*, No. 034306.
- (17) Meyer, F.; Blum, M.; Benkert, A.; Hauschild, D.; Nagarajan, S.; Wilks, R. G.; Andersson, J.; Yang, W.; Zharnikov, M.; Bär, M.; et al. Building-Block Picture” of the Electronic Structure of Aqueous Cysteine Derived from Resonant Inelastic Soft X-Ray Scattering. *J. Phys. Chem. B* **2014**, *118*, 13142–13150.
- (18) Eckert, S.; Niskanen, J.; Jay, R. M.; Miedema, P. S.; Fondell, M.; Kennedy, B.; Quevedo, W.; Iannuzzi, M.; Föhlich, A. Valence orbitals and local bond dynamics around N atoms of histidine under X-ray irradiation. *Phys. Chem. Chem. Phys.* **2017**, *19*, 32091.
- (19) Messer, B. M.; Cappa, C. D.; Smith, J. D.; Drisdell, W. S.; Schwartz, C. P.; Cohen, R. C.; Saykally, R. J. Local Hydration Environments of Amino Acids and Dipeptides Studied by X-Ray Spectroscopy of Liquid Microjets. *J. Phys. Chem. B* **2005**, *109*, 21640–21646.
- (20) Aziz, E. F.; Ottosson, N.; Eisebitt, S.; Eberhardt, W.; Jagoda-Cwiklik, B.; Vácha, R.; Jungwirth, P.; Winter, B. Cation-Specific Interactions with Carboxylate in Amino Acid and Acetate Aqueous Solutions: X-Ray Absorption and Ab Initio Calculations. *J. Phys. Chem. B* **2008**, *112*, 12567–12570.
- (21) Horikawa, Y.; Tokushima, T.; Harada, Y.; Takahashi, O.; Chainani, A.; Senba, Y.; Ohashi, H.; Hiraya, A.; Shin, S. Identification of Valence Electronic States of Aqueous Acetic Acid in Acid–Base Equilibrium Using Site-Selective X-ray Emission Spectroscopy. *Phys. Chem. Chem. Phys.* **2009**, *11*, 8676–8679.
- (22) Gråsjö, J.; Andersson, E.; Forsberg, J.; Duda, L.; Henke, E.; Pokapanich, W.; Björneholm, O.; Andersson, J.; Pietzsch, A.; Hennies, F.; et al. Local Electronic Structure of Functional Groups in Glycine s Anion, Zwitterion, and Cation in Aqueous Solution. *J. Phys. Chem. B* **2009**, *113*, 16002–16006.
- (23) Blum, M.; Odelius, M.; Weinhardt, L.; Pookpanratana, S.; Bär, M.; Zhang, Y.; Fuchs, O.; Yang, W.; Umbach, E.; Heske, C. Ultrafast Proton Dynamics in Aqueous Amino Acid Solutions Studied by Resonant Inelastic Soft X-Ray Scattering. *J. Phys. Chem. B* **2012**, *116*, 13757–13764.
- (24) Weinhardt, L.; Blum, M.; Fuchs, O.; Benkert, A.; Meyer, F.; Bär, M.; Denlinger, J. D.; Yang, W.; Reinert, F.; Heske, C. RIXS Investigations of Liquids, Solutions, and Liquid/Solid Interfaces. *J. Electron Spectrosc. Relat. Phenom.* **2013**, *188*, 111–120.
- (25) Zubavichus, Y.; Shaporenko, A.; Grunze, M.; Zharnikov, M. NEXAFS Spectroscopy of Homopolypeptides at all Relevant Absorption Edges: Polyisoleucine, Polytyrosine, and Polyhistidine. *J. Phys. Chem. B* **2007**, *111*, 11866–11867.
- (26) Stewart-Ornstein, J.; Hitchcock, A. P.; Cruz, D. H.; Henklein, P.; Overhage, J.; Hilpert, K.; Hale, J. D.; Hancock, R. E. W. Using Intrinsic X-ray Absorption Spectral Differences to Identify and Map Peptides and Proteins. *J. Phys. Chem. B* **2007**, *111*, 7691–7699.
- (27) Zubavichus, Y.; Shaporenko, A.; Grunze, M.; Zharnikov, M. Is X-ray Absorption Spectroscopy Sensitive to the Amino Acid Composition of Functional Proteins? *J. Phys. Chem. B* **2008**, *112*, 4478–4480.
- (28) Zubavichus, Y.; Shaporenko, A.; Grunze, M.; Zharnikov, M. NEXAFS Spectroscopy of Biological Molecules: From Amino Acids to Functional Proteins. *Nucl. Instrum. Methods Phys. Res. A* **2009**, *603*, 111–114.
- (29) Weinhardt, L.; Benkert, A.; Meyer, F.; Blum, M.; Hauschild, D.; Wilks, R. G.; Bär, M.; Yang, W.; Zharnikov, M.; Reinert, F.; Heske, C. Local Electronic Structure of the Peptide Bond Probed by Resonant Inelastic Soft X-Ray Scattering. *Phys. Chem. Chem. Phys.* **2019**, *21*, 13207–13214.
- (30) Stöhr, J. NEXAFS Spectroscopy. In *Springer Series in Surface Science*; Springer: Berlin, 2003; Vol. 25.
- (31) Lide, D. R. *CRC Handbook of Chemistry and Physics*; CRC Press: Boca Raton, 2005.
- (32) Seah, M. P. Post-1989 Calibration Energies for X-Ray Photoelectron Spectrometers and the 1990 Josephson Constant. *Surf. Interface Anal.* **1989**, *14*, 488.
- (33) Blum, M.; Weinhardt, L.; Fuchs, O.; Bär, M.; Zhang, Y.; Weigand, M.; Krause, S.; Pookpanratana, S.; Hofmann, T.; Yang, W.; et al. Solid and Liquid Spectroscopic Analysis (SALSA) - A Soft X-ray Spectroscopy Endstation with a Novel Flow-Through Liquid Cell. *Rev. Sci. Instrum.* **2009**, *80*, No. 123102.
- (34) Fuchs, O.; Weinhardt, L.; Blum, M.; Weigand, M.; Umbach, E.; Bär, M.; Heske, C.; Denlinger, J.; Chuang, Y.-D.; McKinney, W.; et al. R. High-Resolution, High-Transmission Soft X-Ray Spectrometer for the Study of Biological Samples. *Rev. Sci. Instrum.* **2009**, *80*, No. 063103.
- (35) Rubensson, J.-E.; Neeb, M.; Biermann, M.; Xu, Z.; Eberhardt, W. Electronic Decay of Vibrationally Selected Core Excited States in Molecular N<sub>2</sub>. *J. Chem. Phys.* **1993**, *99*, 1633–1636.
- (36) Lusvardi, V. S.; Barteau, M. A.; Chen, J. G.; Eng, J.; Frühberger, B.; Tepljakov, A. An NEXAFS Investigation of the Reduction and Reoxidation of TiO<sub>2</sub>(001). *Surf. Sci.* **1998**, *397*, 237–250.
- (37) Watts, B.; Ade, H. A simple method for determining linear polarization and energy calibration of focused soft X-ray beams. *J. Electron Spectrosc. Relat. Phenom.* **2008**, *162*, 49–55.
- (38) Hermann, K.; Pettersson, L. G. M.; Casida, M. E.; Daul, C.; Goursoat, A.; Koester, A.; Proynov, E.; St-Amant, A.; Salahub, D. R.; Carravetta, V. et al. StoBe-deMon Version 3.1, 2011.
- (39) Meyer, F.; Blum, M.; Benkert, A.; Hauschild, D.; Jeyachandran, Y. L.; Wilks, R. G.; Yang, W.; Reinert, F.; Heske, C.; Zharnikov, M.; et al. Site-Specific Electronic Structure of Imidazole and Imidazolium in Aqueous Solutions. *Phys. Chem. Chem. Phys.* **2018**, *20*, 8302–8310.
- (40) Hennies, F.; Pietzsch, A.; Berglund, M.; Föhlich, A.; Schmitt, Th.; Strocov, V.; Karlsson, H. O.; Andersson, J.; Rubensson, J.-E. Resonant Inelastic Scattering Spectra of Free Molecules with Vibrational Resolution. *Phys. Rev. Lett.* **2010**, *104*, No. 193002.
- (41) Weinhardt, L.; Weigand, M.; Fuchs, O.; Bär, M.; Blum, M.; Denlinger, J. D.; Yang, W.; Umbach, E.; Heske, C. Nuclear dynamics in the core-excited state of aqueous ammonia probed by resonant inelastic soft x-ray scattering. *Phys. Rev. B* **2011**, *84*, No. 104202.
- (42) Weinhardt, L.; Benkert, A.; Meyer, F.; Blum, M.; Wilks, R. G.; Yang, W.; Bär, M.; Reinert, F.; Heske, C. Nuclear dynamics and

spectator effects in resonant inelastic soft x-ray scattering of gas-phase water molecules. *J. Chem. Phys.* **2012**, *136*, No. 144311.

(43) Wilks, R. G.; Erbing, A.; Sadoughi, G.; Starr, D. E.; Handick, E.; Meyer, F.; Benkert, A.; Ianuzzi, M.; Hauschild, D.; Yang, W.; et al. M. Dynamic Effects and Hydrogen Bonding in Mixed-Halide Perovskite Solar Cell Absorbers. *J. Phys. Chem. Lett.* **2021**, *12*, 3885–3890.

(44) Wilks, R. G.; MacNaughton, J. B.; Kraatz, H.-B.; Regier, T.; Blyth, R. I. R.; Moewes, A. Comparative Theoretical and Experimental Study of the Radiation-Induced Decomposition of Glycine. *J. Phys. Chem. A* **2009**, *113*, 5360–5366.

(45) Luo, Y.; Ågren, H.; Gel'mukhanov, F. Polarization anisotropy in resonant x-ray emission from molecules. *Phys. Rev. A* **1996**, *53*, 1340.

(46) Horton, H. R.; Moran, L. A.; Scrimgeour, K. G.; Perry, M. D.; Rawn, J. D. *Biochemie - Das Basislehrbuch - Aktuell und Anwendungsorientiert*; Addison-Wesley Verlag: München, 2008.

(47) Fuchs, O.; Zharnikov, M.; Weinhardt, L.; Blum, M.; Weigand, M.; Zubavichus, Y.; Bär, M.; Maier, F.; Denlinger, J. D.; Heske, C.; et al. Isotope and Temperature Effects in Liquid Water Probed by X-ray Absorption and Resonant X-ray Emission Spectroscopy. *Phys. Rev. Lett.* **2008**, *100*, No. 027801.

(48) Blum, M. Electronic and Chemical Properties of Liquids and Solutions, Ph.D. Thesis; University of Würzburg, 2010.

(49) Tokushima, T.; Horikawa, Y.; Harada, Y.; Takahashi, O.; Hiraya, A.; Shin, S. Selective Observation of the Two Oxygen Atoms at Different Sites in the Carboxyl Group (-COOH) of Liquid Acetic Acid. *Phys. Chem. Chem. Phys.* **2009**, *11*, 1679–1682.

(50) Horikawa, Y.; Tokushima, T.; Hiraya, A.; Shin, S. Pronounced Polarization Anisotropy in Resonant X-ray Emission from Acetic Acid Molecules in Solution. *Phys. Chem. Chem. Phys.* **2010**, *12*, 9165–9168.

(51) Hauschild, D.; Seitz, L.; Gharibzadeh, S.; Steining, R.; Jiang, N.; Yang, W.; Paetzold, U. W.; Heske, C.; Weinhardt, L. Impact of N-Butylammonium Bromide on the Chemical and Electronic Structure of Double-Cation Perovskite Thin Films. *ACS Appl. Mater. Interfaces* **2021**, *13*, 53202.

(52) Weinhardt, L.; Ertan, E.; Iannuzzi, M.; Weigand, M.; Fuchs, O.; Bär, M.; Blum, M.; Denlinger, J. D.; Yang, W.; Umbach, E.; et al. Probing Hydrogen Bonding Orbitals: Resonant Inelastic Soft X-Ray Scattering of Aqueous NH<sub>3</sub>. *Phys. Chem. Chem. Phys.* **2015**, *17*, 27145–27153.

## Recommended by ACS

### Mechanism of Mixed-Valence Fe<sup>2.5+...Fe<sup>2.5+</sup> Formation in Fe<sub>4</sub>S<sub>4</sub> Clusters in the Ferredoxin Binding Motif</sup>

Tomoki Kanda, Hiroshi Ishikita, *et al.*

APRIL 18, 2022  
THE JOURNAL OF PHYSICAL CHEMISTRY B

READ 

### Multiconfigurational SCF and Short-Range DFT Combined with Polarizable Density Embedding: Comparison of Linear-Response and State-Specific Solvatochromic Shifts of Acro...

Willem Van den Heuvel, Jacob Kongsted, *et al.*

SEPTEMBER 21, 2022  
JOURNAL OF CHEMICAL THEORY AND COMPUTATION

READ 

### Identification of Valence Electronic States Reflecting the Hydrogen Bonding in Liquid Ethanol

Ryosuke Yamamura, Osamu Takahashi, *et al.*

FEBRUARY 01, 2022  
THE JOURNAL OF PHYSICAL CHEMISTRY B

READ 

### Strong Isotopic Fractionation of Oxygen in TiO<sub>2</sub> Obtained by Surface-Enhanced Solid-State Diffusion

Heonjae Jeong and Edmund G. Seebauer

OCTOBER 17, 2022  
THE JOURNAL OF PHYSICAL CHEMISTRY LETTERS

READ 

Get More Suggestions >